Fatigue fracture mechanisms of Cu/lead-free solders interfaces

Q.K. Zhang, Q.S. Zhu, H.F. Zou, Z.F. Zhang*

Shenyang National Laboratory for Materials Science, Institute of Metal Research, Chinese Academy of Sciences, Shenyang 110016, PR China

ARTICLE INFO

ABSTRACT

In this study the authors present and discuss the results of the investigation on the fatigue fracture behaviors in a series of as-soldered and thermal-aged copper/lead-free solder joints deformed under both monotonic and cyclic loadings. The observation results showed that fatigue cracks generally initiate around the IMC/solder interface when the loading axis is vertical to the interface. The intrinsic deformation behaviors are little different for different solder joints resulting from strain localization induced by the stain mismatch. Fracture surface observations revealed the crack propagation path and fatigue resistance of the solder joints to be affected by the yield strength and mechanical property of the solder. When the copper/solder interface is parallel to the loading axis, the interfacial IMC layer failed approximately perpendicular to the interface when the cumulative strain exceeded the fracture strain, then the cracks propagated to the IMC/solder interface, leading to the fracture along the interface. The failure mechanisms and factors influencing interfacial fatigue are discussed.

© 2009 Elsevier B.V. All rights reserved.

1. Introduction

Lead-rich solders have been widely used in electronics assembly for many years. However, due to the toxicity of Pb, major industrialized countries have legislated to limit their application [1]. As a result of that, many lead-free alloys, mainly consisting of Sn with small additions of other elements such as Ag, Cu, Bi and Sb, have been proposed as the candidates of the Sn–Pb solder [2,3]. Because soldering in the microelectronics industry not only provides the electronic connection, but also ensures the mechanical reliability of solder joints under the complex service conditions, it has been recognized that one of the major concerns for the integrity of the solder interconnection is the adhesive property of the solder/substance interfaces [3]. In particular, with the trend that the solder joints are expected to perform in more dynamic service environments where the stress and strain distributions change with time, not only the tensile or shear properties but also the fatigue resistance of the solder joints become of great significance for electronic reliability [3,4]. Furthermore, the continuing miniaturization of solder joints has set up higher standards for mechanical reliability of the interconnection.

In recent years, there have been many investigations concerning the fatigue properties of the lead-free solders and solder joints [5–17]. However, the correlative data of that available in the literature are still limited and always from different resources, especially for the solder joints. Besides, a comprehensive understanding on the fracture mechanism is also necessary, because the solder joints in application always fail along the soldering interface. In addition, there is a complex evolution of the solder/substrate interface when the solder joints are in service, namely, the growth of interfacial IMC layer and coarsening of the solder's microstructure. Influence of the evolution on the fatigue resistance and failure mechanism of solder joints are also lack of attention.

In the present study, therefore, the authors have concentrated their efforts to reveal the fatigue behaviors of a series of the Cu/lead-free solder joints. Both the as-soldered and thermal-aged interfaces were tested under different orientation of loadings, in order to get a comprehensive understanding on the interfacial fatigue failure mechanisms. Some reliable data of fatigue lives were tested to make a quantitative comparison. The fracture behaviors of as-soldered and thermal-aged solder joints were compared to investigate the influence of thermal aging on that. The lead-free solders used were the SnAg, SnAgCu and SnBi alloys and Cu was chosen as the substrate material. The SnAg and SnAgCu alloy are the promising candidates for the traditional SnPb solder because of their good soldering ability and excellent mechanical properties [18,19], while the SnBi solder is used in low temperature soldering due to its low melting point [20]. Fatigue properties of the Cu/Sn–37Pb solder joints were investigated as reference. The evolution of the microstructure and mechanical properties of the Sn–4Ag and Sn–58Bi solder alloys during aging process were also observed to make a full scale discussion. Based on the experimental results and observations on the interfacial deformation behaviors and fracture surfaces, the failure mechanisms and factors influencing the interfacial fatigue were discussed.

---

* Corresponding author. Tel.: +86 24 23971043; fax: +86 24 23891320.
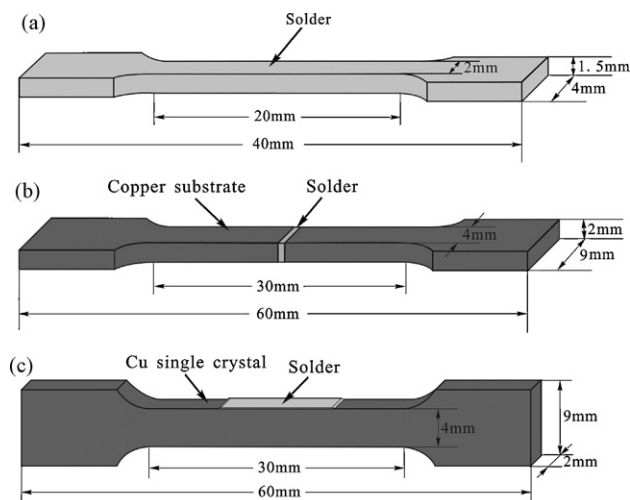 E-mail address: zhfzhang@imr.ac.cn (Z.F. Zhang).

Fig. 1. Configuration of samples and experiments: (a) tensile samples of bulk solder alloy; (b) fatigue samples with loadings vertical and (c) parallel to the Cu/solder interface.

2. Experimental procedure

2.1. Preparation of materials

The Cu substrate material used in this study was prepared from oxygen-free-high conductivity (OFHC) Cu of 99.999% purity by the Bridgman method in a horizontal furnace. The solder alloys chosen were Sn–4Ag (wt%), Sn3.8Ag0.7Cu (wt%) and Sn–58Bi (wt%) solder alloys, the Sn–37Pb solder was used as a reference. All the solder alloys were prepared by melting high purity (>99.99%) tin and Ag, Bi, Pb and Cu at 800 °C for 2 h in vacuum, the smelting process was operated by a vacuum furnace with the maximum heating temperature of 1600 °C.

2.2. Tensile tests of bulk solders

To investigate the influence of thermal aging on the tensile properties of solders, the air-cooled Sn–58Bi and Sn–4Ag bulk solder alloys were cut into standard tensile samples (see Fig. 1(a)), aged at 120 and 180 °C for different times and the side-surfaces were ground with 2000# SiC abrasive paper. The tensile tests were performed with an Instron E1000 fatigue testing machine under a strain rate of $1.25 \times 10^{-4}\,s^{-1}$ at 20 °C in air. Three samples were tested at the same condition to get an average of strength.

2.3. Fatigue tests with loading axis vertical to the interface

The Sn–4Ag, Sn–58Bi and Sn–37Pb solders were used for the solder joints. The joint was formed by reflow soldering and sandwiched between two Cu plates. The surfaces of the Cu plates for soldering were firstly polished with a diamond polishing agent, then a soldering paste was dispersed on the polished area and a solder alloy sheet was placed on the paste to ensure sufficient wetting reaction. The prepared samples were kept in an oven at a constant temperature for a few minutes and then cooled down

in air. Some of the soldered samples were isothermally aged for different times. The reflowing, aging temperatures and times are listed in Table 1. After that, both the as-reflowed and aged samples were spark-cut into fatigue specimens, and the side-surfaces were ground and carefully polished with 1 μm diamond powder for microstructural observations of the Cu/solder interface. The dimensions of the finished fatigue specimens are presented in Fig. 1(b). The stress-controlled fatigue tests were carried out with an Instron 8871 fatigue testing machines under a symmetrical sinusoid waveform ($R = -1$) with a frequency of 2 Hz. The fatigue lives of samples were tested at different stress amplitudes and three samples were tested under the same conditions. The stress amplitude was increased until the fatigue life decreased to about 10^3 cycles. For some samples, cyclic deformation was interrupted at different cycles, and then the interfacial deformation and cracking behaviors were observed with a LEO super35 scanning electronic microscope (SEM) to reveal the interfacial deformation behavior and fatigue fracture mechanisms.

2.4. Fatigue tests with loading axis parallel to the interface

The samples were prepared by depositing a layer of solders on the Cu single crystal. The solders used were the Sn3.8Ag0.7Cu and Sn–58Bi solders. Some Cu blocks were spark-cut from the Cu single crystal plate. By the X-ray Laue back-reflection method, the orientation of the specimen along the loading direction in the present study was determined as [$\bar{1}\,6\,8$]. Before the reaction of molten solder with Cu single crystal, the Cu surface was electro-polished carefully. The next reacting process is similar to the process mentioned in Section 2.3. The reflowing, aging temperatures and times are also listed in Table 1. Then the Cu blocks were cut into standard samples with a thickness of 3 mm. The configuration of the final testing sample is presented in Fig. 1(c). Before fatigue tests, the side-surfaces of specimens were carefully polished for interfacial microstructure observations. The push–pull strain-controlled fatigue tests were performed on a Shimadzu servo-hydraulic fatigue testing machine at a constant axial plastic strain amplitude of 10^{-3} at 20 °C in air. Cyclic deformation was also interrupted at different cycles, for the observations of the interfacial deformation and cracking behaviors to reveal the fracture mechanisms.

3. Results and discussion

3.1. Evolution of interfacial morphology and mechanical properties of solders

The evolution of the interfacial morphologies of the Sn–4Ag/Cu and Sn–58Bi/Cu interfaces during aging process is shown Fig. 2. For the as-soldered SnAg/Cu interface, a layer with scallop-like morphology was formed along the interface, as shown in Fig. 2(a). EDX analysis indicates that the layer is the Cu_6Sn_5 intermetallic compound. It was also found that the microstructure of the Sn–4Ag solder is composed of Sn matrix and Ag_3Sn "particles", the particles are in fact needle-like Ag_3Sn grains [21]. After aged at 180 °C for 4 days, the IMC layer increased and the IMC/solder interface became evidently flat (see Fig. 2(b)). Meanwhile, the IMC layer changed into a duplex layer, and the new interfacial IMC phase was identified to

Table 1
Reflowing, aging temperatures and times of different solder joints.

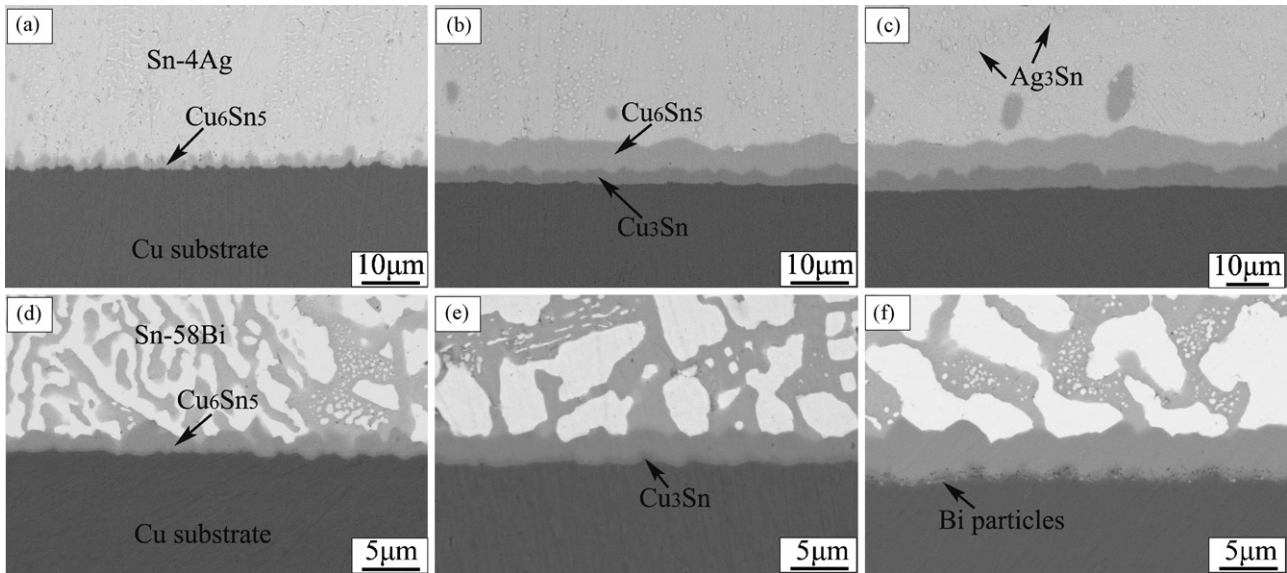| Solder joints	Reflowing temperature (°C)	Reflowing time (min)	Aging temperature (°C)	Aging time (day)
Sn–4Ag/Cu	260	5	180	4, 16
Sn–37Pb/Cu	220	5	160	7
Sn3.8Ag0.7Cu/Cu	240	5	170	7
Sn–58Bi/Cu	200	3	120	4, 7, 9

Fig. 2. Interfacial microstructure of the SnAg/Cu solder joints: (a) as-soldered, (b) aged for 4 days, (c) aged for 16 days and SnBi/Cu solder joints: (d) as-soldered, (b) aged for 4 and (f) 9 days.

be Cu_3Sn. For the samples aged for 16 days, the IMC layer morphology changed little, as in Fig. 2(c), only the thickness doubled. Compared the microstructure of the as-reflowed and aged solder, a coarsening trend of the needle-like Ag_3Sn particles was observed, which can in turn affect the mechanical properties of the solder alloy [22]. The morphology of the as-soldered SnBi/Cu interface is exhibited in Fig. 2(d). An interfacial IMC layer, confirmed to be Cu_6Sn_5 phase by EDS analysis, was observed between the Cu substrate and the SnBi solder. After aged at 120 °C for 4 days, the IMC layer became evidently thick, and a very thin Cu_3Sn layer appeared between the Cu substrate and the Cu_6Sn_5 (see Fig. 2(e)). Moreover, noticeable coarsening of the Sn–Bi eutectic microstructure was also observed, which may in turn affect the mechanical properties of solder. The interfacial morphology of the sample aged for 9 days is shown in Fig. 2(f). It is obvious that the IMC thickness increased a bit, while the alteration of the interfacial morphology and the microstructure of solder are little. In addition, some discontinuous Bi particles (the bright spots) were observed at these long-term aged IMC/Cu interfaces. That will induce an embrittlement of the interface [23]. However, the difference in microstructures of the aged solder alloy is not significant, indicating that the coarsening of solder alloy may occur only at the early stage of aging.

As the microstructure of the solder coarsening during the aging process, it is necessary to investigate its influence on the mechanical properties of the solders. Evolution on tensile strength of the Sn–4Ag and Sn–58Bi solder alloys during the aging process are shown in Fig. 3. It is obvious that the Sn–58Bi solder has much higher yield strength than the Sn–4Ag solder at the current strain rate. Moreover, though there is obvious coarsening on microstructure of the solders, the decrease in tensile strength is slight and
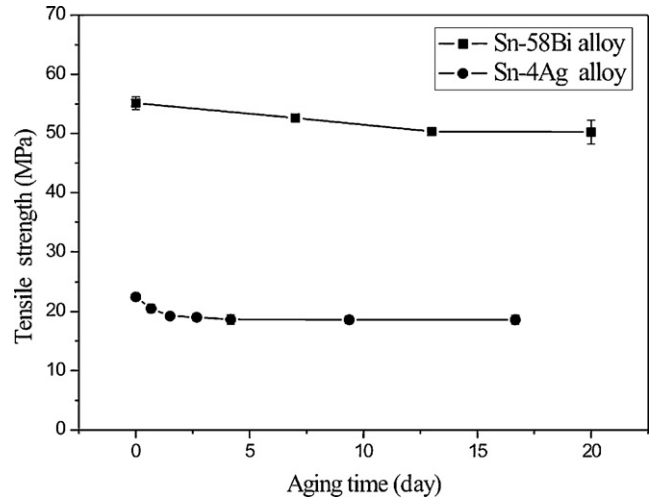

Fig. 3. Evolution of tensile strength of the Sn–4Ag and Sn–58Bi solder alloy during aging process.

becomes steady at the later aging process. That is consistent with the observation results on microstructure of solder alloys and some reports before [22]. The data available in literature for mechanical properties of the SnAg, SnBi and SnPb solders are summarized in Table 2 for Refs. [24–28]. As the mechanical properties of the solder alloys are affected by the microstructure, strain rate and testing temperature [18,29], the data from various sources are a little bit different. In general, it is recognized that the SnAg and SnAgCu

Table 2
Mechanical properties of solder alloys.

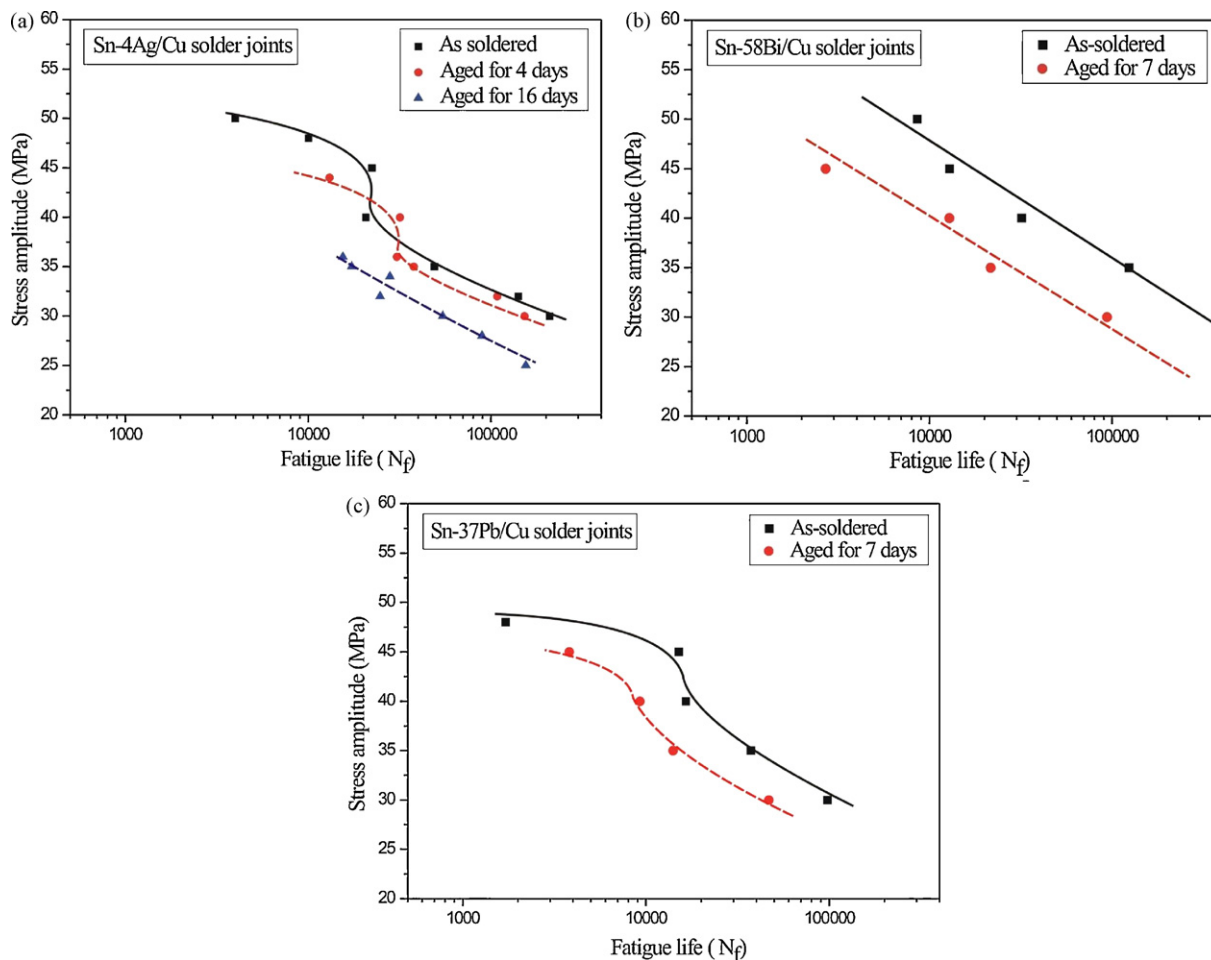| Solder alloys	Elastic modulus (GPa)	Reference	UTS (MPa)	Reference	Percent elongation (%)	Reference
Sn–3.5Ag	50	[24]	55 at 0.022 strain rate, cast Processing 37 at 0.000033 strain rate, cast Processing 20 at 0.00015 strain rate, cast Aged 25 °C	[24]	35	[25]
Sn–37Pb	39, 30.5		19 at 20 °C	[26]	35–176	[27]
Sn–58Bi	42		45–80	[28]	40–200	[28]

Fig. 4. S–N relationship of SnBi/Cu, SnPb/Cu and SnAg/Cu solder joints.

solders have good ductility, but their UTS is a little bit low at low strain rate; while the SnBi solder has high UTS, good ductility at low strain rate, but displays quite brittle feature at high strain rate [24–29].

It has been acknowledged that the tensile property of the Sn–based solder is substantially influenced by the strain rate, the relationship between the tensile strength of solder and the strain rate can be expressed by a power-type equation [29,30]:

$$\sigma = C\dot{\varepsilon}^m \tag{1}$$

where σ is the tensile strength, $\dot{\varepsilon}$ is the strain rate, m is the strain rate sensitivity and C is a constant. In the fatigue tests, the strain rate is very high. Therefore, the solder will exhibit higher strength during the fatigue test. In this study, the solders in the joints only showed a little plastic deformation at some special location during the fatigue test though the stress amplitude was around the range of 30–50 MPa, which will be referred later in this paper.

3.2. Fatigue damage behavior of Cu/solder interfaces vertical to loading

3.2.1. S–N relationship of solder joints

Fig. 4 shows the relationship between the stress amplitude and fatigue life of the as-soldered and aged Sn–4Ag/Cu, Sn–58Bi/Cu and Sn–37Pb/Cu solder joints, all the three figures have the same coordinates to make an intuitionistic comparison in fatigue lives. In general, it is found that both the SnBi/Cu and SnAg/Cu solder joints have a slight higher fatigue resistance than the SnPb/Cu

solder joints, and the fatigue lives decrease after aging for a few days. However, the evolution of fatigue lives with increasing stress amplitude is a bit complex and different for different solder joints. The fatigue damage mechanisms will be discussed later in this paper in combined with the interfacial deformation behavior and fracture surfaces.

For the as-soldered Sn–4Ag/Cu solder joints, the fatigue lives display an approximately exponential increase with decreasing stress amplitude at low stress amplitude, while there is a nearly upright ascent in fatigue lives when the stress amplitude is around 40–45 MPa. Five samples were tested at 45 MPa to confirm such phenomenon. In fact, similar phenomena have been also observed for the lead-rich solder under isothermal fatigue loadings [31]. It was also reported that there is a transition in crack propagation mechanism when the strain is up to a critical value for the Sn3.5Ag solder [8]. Because the yield strength of Sn–4Ag solder is about 40–50 MPa at the current strain rate [18,24], that may be caused by yielding of the solder. The solder joints aged for 4 days exhibit a similar S–N curve, but have a lower turning point, due to the decrease in the yield strength of solder. The solder joints aged for 16 days never show such phenomenon because the applied stress amplitudes on them were lower than the yield strength of solder. The S–N curves of the SnPb/Cu solder joints are very similar to that of the SnAg/Cu joints, only a bit lower in fatigue lives.

For both the as-soldered and aged SnBi/Cu solder joints, the fatigue life also displays an approximately exponential increase with decreasing stress amplitude. It has been reported that the SnBi/Cu solder joints have low fatigue resistance because of the
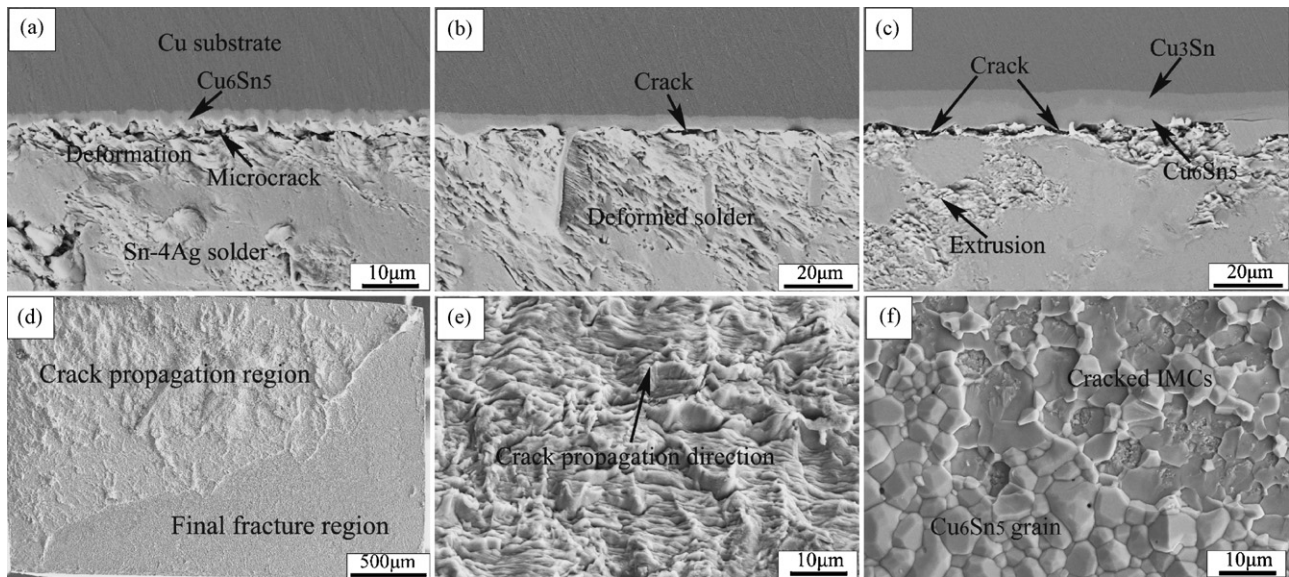
Fig. 5. Interfacial deformation behavior and fatigue fracture morphologies of the Sn–4Ag/Cu solder joints: (a) as-soldered sample, $\sigma_a = 35$ MPa, $N = 10^4$; (b) sample aged for 4 days, $\sigma_a = 35$ MPa, $N = 10^4$; (c) aged for 16 days, $\sigma_a = 30$ MPa, $N = 10^4$; (d) fatigue fracture surface; (e) microstructure of crack propagation region and (f) final fracture region.

inferior ductility of the SnBi solder [20], whereas, the results in this study show that they have comparable fatigue resistance than the SnAg/Cu solder joints at the same stress amplitude. Though the solders have poor ductility, the higher tensile strength of the SnBi/Cu solder joints conceals that shortage to some extent at low stress amplitude, making their fatigue resistivity comparable with the SnAg/Cu solder joints. Even so, as the SnBi/Cu solder joints have much higher fracture strength than the SnAg/Cu joints, they do have poor fatigue resistance at the same stress ratio (σ_a/σ_f). The SnBi/Cu solder joints did not exhibit an upright ascent phenomenon because the applied stress amplitude is far below the yield strength of the solder and the curves may never reach the turning point. In addition, the decrease in fatigue life of the SnBi/Cu solder joints after aging is much obvious. After aging for 9 days, the SnBi/Cu solder joints exhibited a totally brittle feature.

3.2.2. Fatigue fracture behaviors of solder joints

The fatigue deformation behaviors and fracture surfaces of the Sn–4Ag/Cu solder joints are shown in Fig. 5. As the solder joints deformed at different stress amplitude exhibited similar fracture behavior, one sample is chosen as example for each aging time. Fig. 5(a) shows the interfacial morphology of an as-soldered sample deformed at the stress amplitude of 35 MPa for 10^4 cycles, in which the deformation of the solder close to the IMC/solder interface is serious and microcracks were observed at the interface. The sample aged for 4 days and deformed for 10^4 cycles at 35 MPa is shown in Fig. 5(b); it was found that the interfacial deformation and crack initiation behavior of the solder joints changed little after aging for 4 days. Fig. 5(c) shows the deformation morphology of the sample aged for 16 days and deformed for 10^4 cycles at 30 MPa. Though the IMC layer was much thicker and there was certain coarsening of the solder, it is notable that the deformation behavior changed
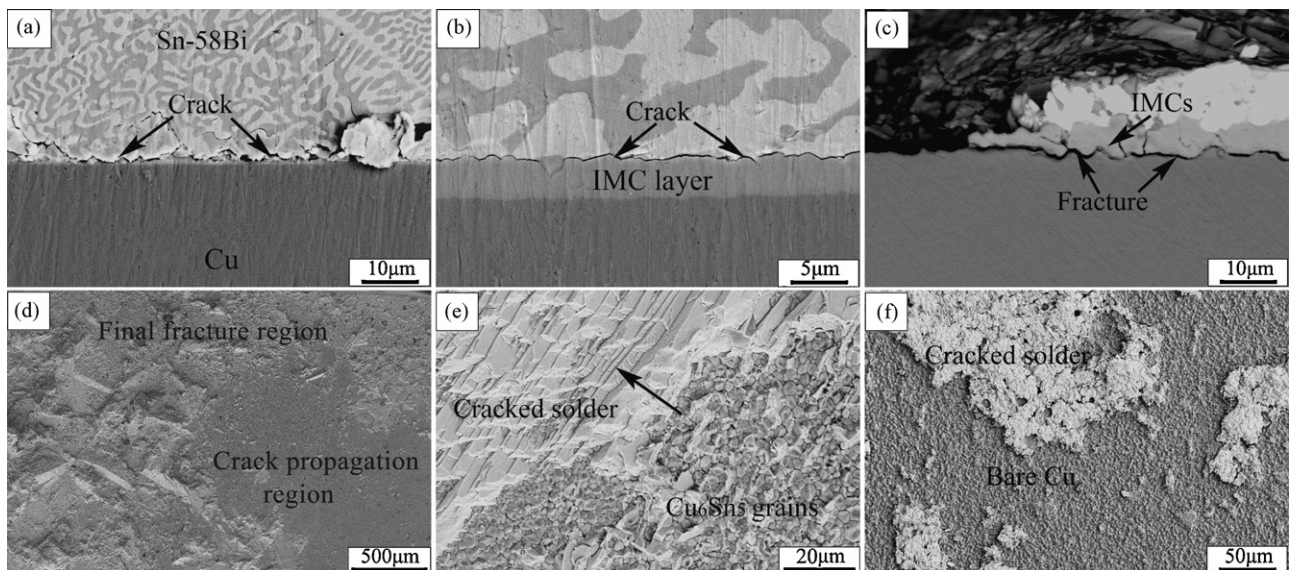

Fig. 6. Fatigue cracks initiation behavior and fracture morphology of Sn–58Bi/Cu interfaces: (a) as-soldered sample, $\sigma_a = 50$ MPa, $N = 5000$; (b) sample aged for 7 days, $\sigma_a = 35$ MPa, $N = 2 \times 10^4$; (c) side-surface of samples aged for 9 days; (d) macroscopic fatigue fracture surface and (e) microstructure of crack propagation region of samples aged for 7 days; (f) fracture surface of sample aged for 9 days.
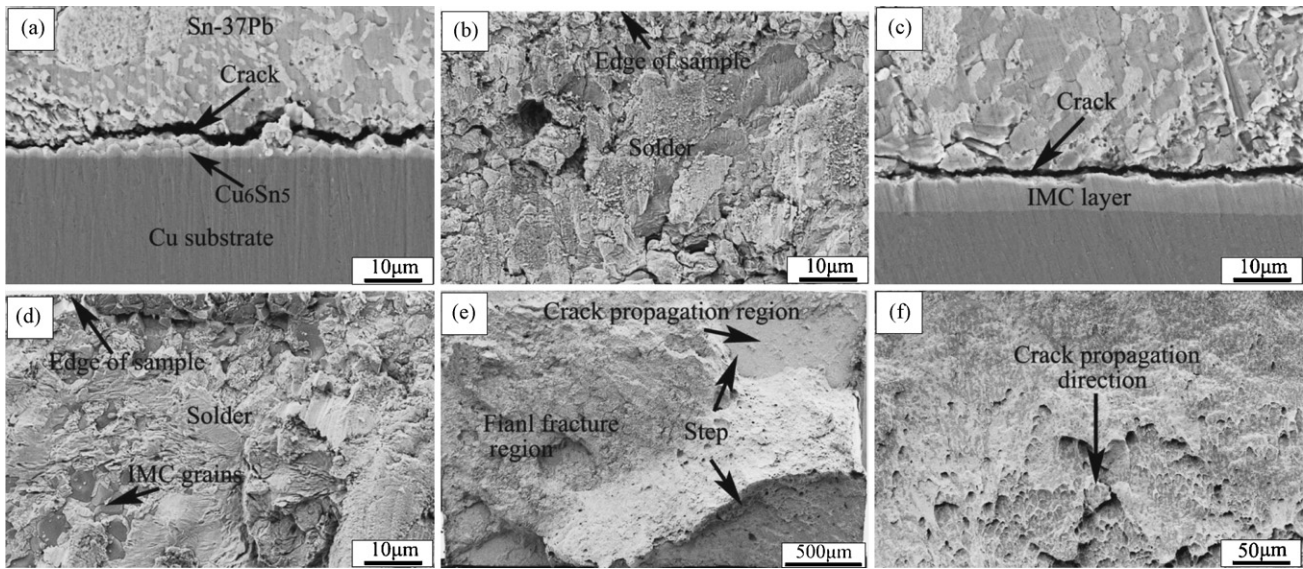
Fig. 7. Fatigue cracks initiation behavior and fracture morphology of Sn–37Pb/Cu interfaces: side-surface of (a) as-soldered sample, $\sigma_a = 45$ MPa, $N = 7000$; (b) fracture morphology at the edge of as-soldered sample; (c) aged sample, $\sigma_a = 35$ MPa, $N = 10^4$; (d) fracture morphology at the edge of aged sample; (e) macroscopic and (f) microscopic image of fracture surface.

little and microcracks still initiated along the IMC/solder interface. In addition, though there are intrusions and extrusions of solder, however, they do not evolve into primary fatigue cracks. For all the SnAg/Cu solder joints, the fractures are very similar. Based on that, it can be concluded that the solder joints aged for different times have similar deformation behavior and crack initiation mechanism. As the solder joints are far from being a homogeneous structure, the deformation of solder is not homogeneous and the solder close to the interface deforms much severe. In fact, the simulation of Von Mises stress distribution inside the solder joint had shown a singular phenomenon at the solder interface, which is due to the strain mismatch among the Cu substrate solder alloy and IMC layer [32]. Typical fatigue fracture surface consists of two regions, as shown in Fig. 5(d). The first region is rough and covered by some deformed solder, a trace of crack propagation can still be observed on microscale (see Fig. 5(e)) though the SnAg solder has good ductility. Investigation on fatigue crack propagation behavior of the SnAg solder has confirmed that cracks propagated in a transgranular manner at high strain [7]. According to the morphology of crack propagation region, it can be concluded that the crack also propagated in a transgranular manner for the solder joints. The second region is flat and covered by the cracked IMCs (see Fig. 5(f)), which is similar to the fracture surface of the solder joints at high strain rate [33]. Therefore, it is reasonable to consider that it is the final fracture region. Based on the observation results above, the fatigue fracture processes can be predicated as follows: under cyclic loadings, the solders close to the Cu_6Sn_5/solder interface deforms severely on account of the stress concentration. With increasing cyclic number, microcracks appear at the solder/IMC interface, link to form long cracks and propagate inside the solder close to the interface in a transgranular manner. The effective loading area reduces and the real stress applied on the solder joints increases with propagation of fatigue cracks. When the real stress approaches to the fracture strength of the solder joints, final brittle fracture occurs.

Fig. 6 shows the deformation behavior and fracture surfaces of the Sn–58Bi/Cu solder joints, also one sample is chosen as example for each aging condition. The interfacial morphology of the as-soldered sample deformed at 50 MPa for 5000 cycles is shown in Fig. 6(a), in which long fatigue crack was observed along the solder/IMC interface. Due to the high yield strength of the SnBi alloy, the deformation of the solder close to the solder/IMC inter-

face is quite slight. Fig. 6(b) shows the interfacial morphology of the sample aged for 7 days and deformed at 35 MPa for 2×10^4 cycles. Though the coarsening of the solder was obvious and the interfacial IMC layer was much thicker, fatigue crack still initiated exactly along the solder/IMC interface. However, the solder joints aged for over 9 days fractured along the IMC/Cu interface at very low stress amplitude, as shown in Fig. 6(c), accompanying with a sharp decrease in fatigue life. The essential transition in fracture mechanism of the long-term aged SnBi/Cu solder joints is induced by the interfacial Bi segregation [23]. Fig. 6(d) shows the typical fatigue fracture surface of the SnBi/Cu solder joints prior to the occurrence of brittle fracture, which is also composed of two regions. The first region is covered by some perfect Cu_6Sn_5 grains, with little residual solders, as shown in Fig. 6(e). In contrast, the microscopic morphology of the second region is covered by a thin layer of cracked solder, the same as the tensile fracture surfaces of the solder joints [34], thus it is considered to be the final fracture region and the former one is the crack propagation region. It can be therefore concluded that for the SnBi/Cu solder joints, the fatigue cracks initiate and propagate along the solder/Cu_6Sn_5 interface and finally fracture inside the solder close to the interface. The fracture surface of the long-term aged sample is mainly the exposed Cu, with a little cracked solder remnants (see Fig. 6(f)), which is consistent well with the side-surface observation results.

The fatigue damage behavior of the Sn–37Pb/Cu solder joints is shown in Fig. 7. Fig. 7(a) shows the interfacial morphology of an as-soldered sample deformed at 45 MPa for 7000 cycles, it can be found that crack initiated inside the solder close to the solder/IMC interface. The edge of the fracture surface of the as-soldered sample is covered by deformed solder, as in Fig. 7(b), indicating that cracks propagate into the solder near the solder/IMC interface once it forms. Similar to the SnAg/Cu solder joints, the crack initiation mechanism should be also induced by the strain localization, but become easier as the Sn–37Pb solder has low yield strength and superior ductility. After aging for 7 days, there is little change in fatigue failure mechanism. According to Fig. 7(c) and (d), crack still initiates and propagates inside the solder, but seems to be more close to the solder/IMC interface, because IMC grains were observed at the edge of fracture surface. It is therefore concluded that the crack initiation behavior of the SnPb/Cu solder joints is similar to that of the SnAg/Cu joints in general. However, the fatigue fracture

surfaces are a bit different. As shown in Fig. 7(e), the macroscopic view of the fracture surface of the SnPb/Cu interface is rough and fracture step is observed, indicating that the fatigue cracks propagate into the solder along a special angle during the propagate process. The final fracture is a step fracture. The crack propagation region extends from the edge of the sample to the fracture stage. Fig. 7(f) shows the microscopic view of the interface of the two regions; it appears that the crack propagation region is covered by a thin layer of deformed solder, while dimples were observed at the final fracture region. It is therefore predicated that the fatigue cracks propagate inside the solder and the final fracture occurs inside the solder in a dimple mode due to its superior ductility [26,27].

3.2.3. Fatigue fracture mechanisms and influencing factors of fatigue resistance

The fatigue fracture processes of different Cu/solder interfaces vertical to the loadings are summarized in Fig. 8. For a typical fatigue fracture, the fatigue fracture processes consist of the crack initiation and propagation stages. According to the foreside discussion, for all the solder joints, microcracks initiate around the solder/IMC interface on account of the strain localization. The deformation mismatch between solder and the interfacial IMC layer is the essential reason of fatigue crack initiation. However, the propagation paths are a little bit different, affected by the mechanical properties of solder, as illustrated in Fig. 8(a)–(c). For the Sn–4Ag and Sn–37Pb solder joints, crack propagates inside the solder close to the solder/IMC interface, while fatigue cracks of the SnBi/Cu joints propagate exactly along the interface before the interfacial embrittlement occurs. During crack propagation process, the effective loading area reduces and the real applied stress of the solder joints increases with increasing cyclic number, when the real stress approaches to the fracture strength of solder joints, final fracture

occurs. The final fracture modes are similar to the solder joints fracture at high strain rate, affected by the mechanical properties of solder and the interfacial IMC.

Based on the discussion on fatigue fracture processes above, the influencing factors of the fatigue resistance at the two stages are predicted. It is widely accepted that high ductility enhances the low-cycle fatigue resistance of a material [35], but the ductility is not the only influencing factor on fatigue resistance. For a typical fatigue fracture, the fatigue life (N_f) consists of the crack initiation (N_i) and propagation cycles (N_p). For the solder joints, as the crack initiation process is induced by local plastic deformation of solder, the initiation cycles (N_i) are affected by the yield strength of solder. With higher yield strength, the solder is too rigid to deform and microcracks are difficult to initiate, thus the SnBi/Cu solder joints should have higher N_i than the SnAg/Cu and SnPb/Cu solder joints at low stress amplitude. For the SnAg/Cu and SnPb/Cu solder joints, crack propagates inside the solder; a plastic deformation region was formed at the tip of crack. Therefore, the deformation energy of the solder alloy, as the resistance to crack propagation, is the dominative factor to the crack propagation cycles. As the SnAg solder has higher fatigue resistance than the SnPb solder [36], accordingly, the SnAg/Cu solder joints have higher N_p than the SnPb/Cu joints. Though the SnBi solder also has good ductility [28], it shows little plastic strain at the low stress amplitude. Observation on the fracture surface of the SnBi/Cu joints has proved that the fatigue crack propagated along the solder/IMC interface. Because the plastic deformation of the SnBi solder near the interface is slight and the IMC cannot exhibit any plastic deformation, the resistance to crack propagation is low. Therefore, the SnBi/Cu joint sample should have high propagation rate and low propagation cycles. Fig. 8 also gives a simple description on the fracture process of the three solder joints and makes a comparison on their crack initiation, propagation rate and fracture strength. The x-axis is the fatigue cycles and the y-axis
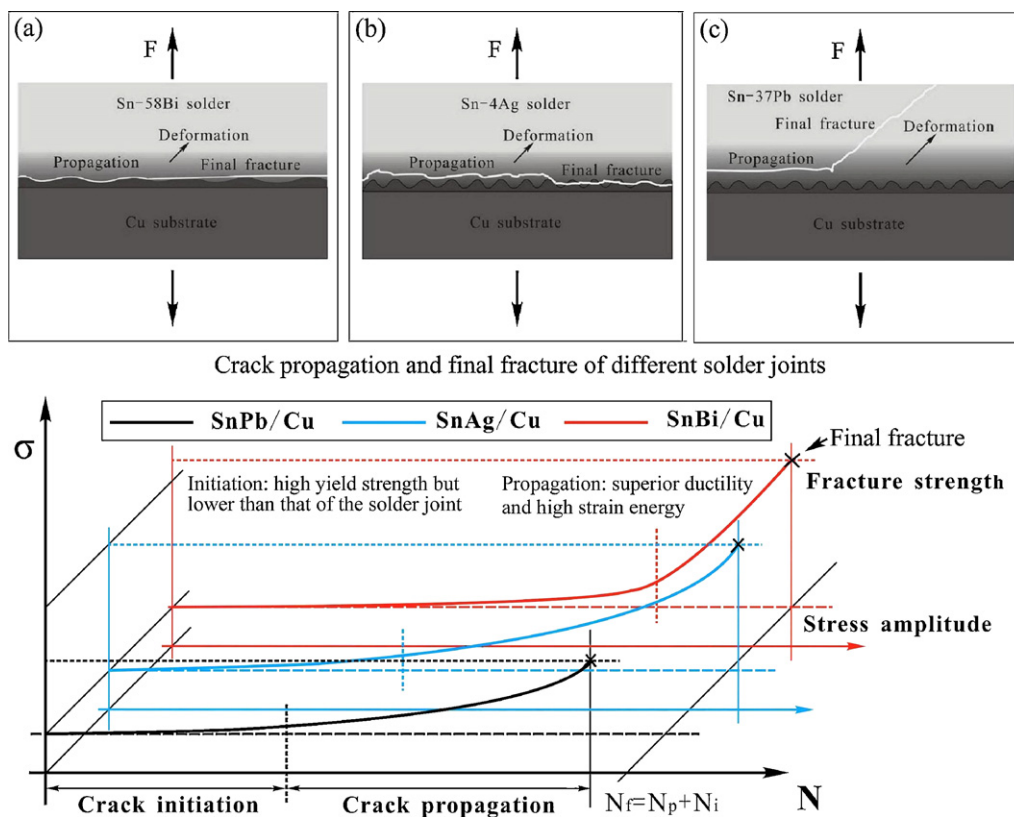

Fig. 8. Illustration of the fatigue fracture mechanisms of Cu/solder joints under loadings vertical to the interface and dominative factors of fatigue resistance: (a)–(c) fatigue crack propagation paths.
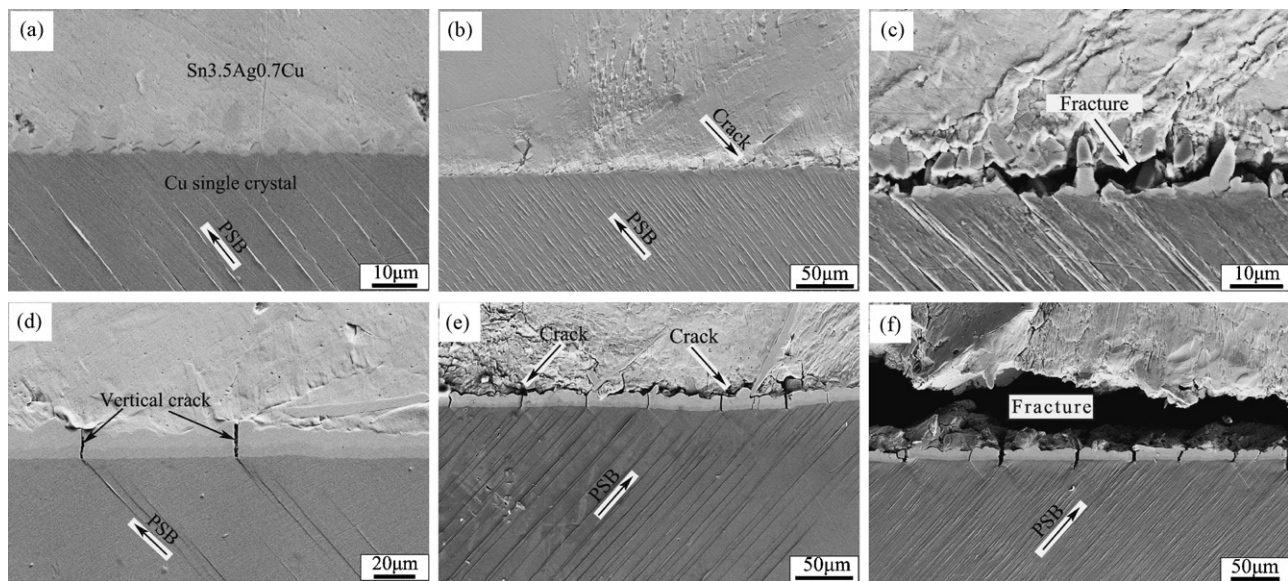
Fig. 9. Fatigue damage behavior of Sn3.8Ag0.7Cu/Cu single crystal interfaces under a plastic strain amplitude of 10^{-3}: interfacial morphology the as-reflowed sample deformed for (a) 650 cycles, (b) 3000 cycles and (c) 4000 cycles; and the sample aged for 7 days deformed for (d) 200 cycles, (e) 2000 cycles and (f) 3000 cycles.

is the real stress, the three lines represent the real stress of the three different solder joints. The real stress increases from the stress amplitude to the fracture strength during the crack initiation and propagation process. As in the figure, the SnPb/Cu joints have the lowest fracture strength and fatigue life at the same stress amplitude. The SnBi/Cu solder joints have the highest fracture strength and N_i, but low N_p, because of their high crack propagate rate. The SnAg/Cu joints have a balance distribution of N_i and N_p. It is well known that the fracture strength of solder joints is affected by the interfacial microstructure [30–34]. From Fig. 8 it is obvious that the propagation cycles also depend on the fracture strength, thus the interfacial structure and the IMC layer can affect the fatigue life by dominating the fracture strength [16]. In addition, for all of the three solder joints, the IMC thickness keep increasing with increasing aging time, but the IMC layer never fractures the crack initiation process, thus the IMC thickness may have little influence on crack initiation mechanism. Besides, though there is obvious coarsening of the solders during the aging process, the decrease in yield strength of them is very slight. Because the stress localization is induced by the deformation mismatch between the solder and IMC layer, the coarsening does not induce an essential transition on crack initiation mechanism though it may affect the crack propagation rate a little.

3.3. Fatigue crack behavior of Cu/solder interfaces parallel to loading

3.3.1. Sn3.8Ag0.7Cu/Cu single crystal interface

Fig. 9 shows the damage behavior of the SnAgCu/Cu single crystal interface parallel to the cyclic loading. For the as-soldered sample deformed for 650 cycles, some persistent slip bands (PSBs) were observed at the surface of the Cu single crystal, as shown in Fig. 9(a). After 2000 cycles, the PSBs became wider and thicker (Fig. 9(b)), indicating that the plastic deformation of the Cu substrate increased with increasing cyclic number. In addition, the plastic deformation of the solder close to the interface is obvious and some microcracks initiated inside the scallop-like interfacial IMC layer. After 4000 cycles, the microcracks linked up and induced fracture between the solder and the Cu substrate, as shown in Fig. 9(c). The fatigue damage behavior of the aged samples is a little bit different from the as-soldered one. Fig. 9(d) shows the inter-

facial morphology of a sample aged for 7 days and deformed for 200 cycles, it is found that the IMC layer had cracked perpendicular to the interface though the plastic deformation of solder was little, because the IMC layer became thick and brittle after aging [32]. After deformed for 2000 cycles, the plastic deformation of both the solder and the Cu substrate increased, and there is a long crack along the solder/IMC interface, as shown in Fig. 9(e). After 3000 cycles, the solder and the Cu substrate had completely broken away (see Fig. 9(f)). According to the observations above, it is predicated that during cyclic deformation, the cracks firstly nucleated perpendicular to the interfacial IMC layer and formed some microcracks, and then the cracks propagated into the IMC/solder interface, link to each other, resulting in the fracture along the solder/IMC interface. For the as-soldered interface, the vertical cracks are not obvious, thus it appears that the vertical cracks and the interfacial cracks initiate synchronously.

3.3.2. Sn-58Bi/Cu single crystal interface

The deformation and fracture behaviors of the as-soldered and aged Sn–58Bi/Cu interfaces at a constant axial plastic strain amplitude of 10^{-3} are exhibited in Fig. 10. Fig. 10(a) shows the interfacial morphology of an as-soldered sample deformed for 3000 cycles. Because of the high yield strength of the SnBi solder, the plastic deformation of the solder was very little. Some microcracks were observed at the solder/IMC interface, but there was no crack of the interfacial IMC layer because the as-soldered sample is rigid. Comparing Fig. 10(a) with Fig. 9(b), it seems that the SnBi/Cu interface has higher fatigue resistance than the SnAgCu/Cu interface in this case. Fig. 10(b) shows the interfacial morphology of the sample aged for 4 days and deformed for 2000 cycles, in which the plastic deformation of the solder is very little but there had been some cracks of the IMC layer. After 6000 cycles, the cracks had evolved into fracture along the solder/IMC interface, while the plastic deformation of the solder is still very little (see Fig. 10(c)). For the long-term aged SnBi/Cu solder joints, there is also an essential transition in the fracture mechanism. As in Fig. 10(d), the SnBi/Cu interface aged for 9 days fractured along the IMC/Cu interface after only 300 cycles, which is similar to that shown in Fig. 6(c) and was also induced by the interfacial Bi segregation [14,23]. As the Bi segregation problem during aging process has become a fatal drawback for the wide application of the Bi-contained solder, studies in attempt to heal or
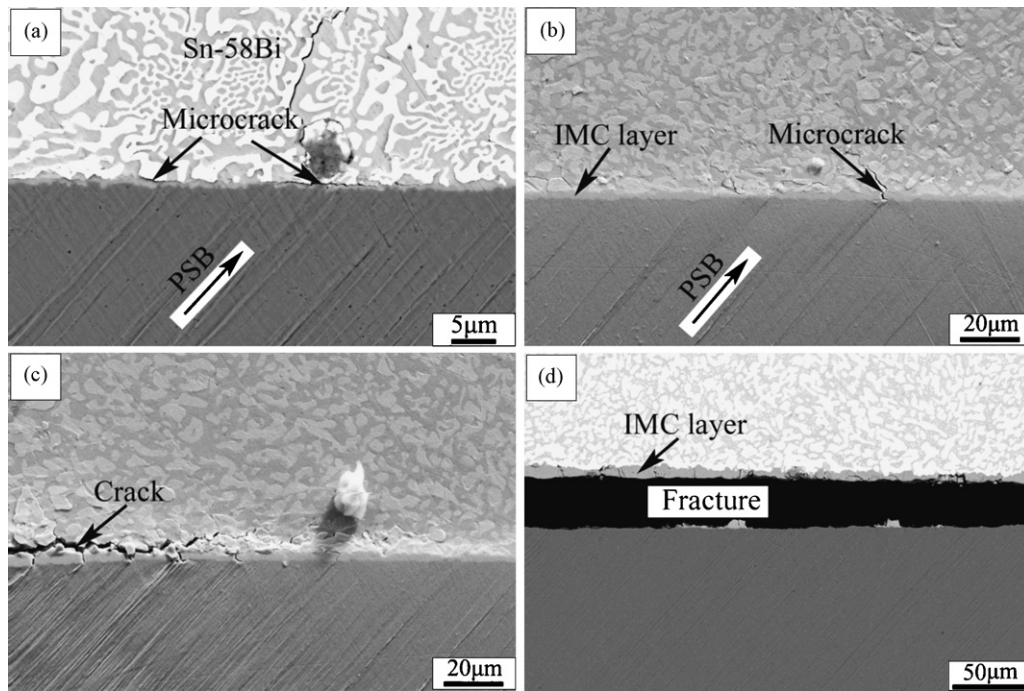
Fig. 10. Fatigue damage behavior of Sn–58Bi/Cu single crystal interfaces under plastic strain amplitude of 10^{-3}: (a) as-reflowed sample, deformed for 3000 cycles; aged for 4 days deformed for (b) 2000 cycles and (c) 6000 cycles; and (d) aged for 9 days deformed for 300 cycles.

alleviate the interfacial Bi segregation under both monotonic and cyclic loadings are in trial [34].

3.3.3. Fatigue cracking mechanism of Cu/solder interface parallel to loading

Based on the observations and discussions before, the fatigue cracking mechanisms of Cu/solder interface parallel to loading are concluded as follows: under constant axial plastic strain amplitude, the Cu substrate, IMC layer and the solder deform synchronously, their total strains keep increasing with cyclic number. Normally the IMC layer can not exhibit any plastic deformation because it is very brittle, when the cumulative plastic strain exceeds to the maximum elastic strain of the IMC layer, it will fracture and some vertical cracks were easily formed with respect to the interface, as illustrated in Fig. 11. With increasing cyclic number, the vertical cracks enlarge, propagate to the IMC/solder interface and link up into a single stretch, resulting in a fracture along the IMC/solder interface (see Fig. 11). As the plastic deformation of the solder is driven by the Cu substrate, the interfacial fracture will decrease the deformation-delivery ability and result in a further fracture. It is noticed that some cracks of the interfacial IMC layer correspond to the outcrop of the PSBs [17], thus the PSBs may be a secondary inducement of the cracking of IMCs. According to the fracture processes above, it can be predicated that the cracking behavior of the IMC layer is mainly influenced by its brittle feature, and the thickness. It is also the decisive factor on the fatigue resistance of the solder interfaces in this case. In addition, though the deformation of the solder near the interface was serious, it has little influence on crack initiation mechanism. Moreover, the mechanical properties and microstructure of the solder have little effect on crack imitation process under this condition. The IMC layer becomes thicker and much brittle during aging process, making the fatigue resistance decrease with increasing aging time.

4. Conclusions

Fatigue fracture behaviors of the as-soldered and aged Cu/lead-free solder joints under monotonic and cyclic loadings were systematically investigated and compared in this study. Based on the experimental results, the following conclusion can be drawn:

(1) Under vertical loading, there is certain strain localization at the solder/Cu interface due to the deformation incompatibility, microcrack always initiates along the solder/Cu interface, while the propagation path depends on the ductility of the solder. Cracks propagate inside the solder close to the interface in the SnAg/Cu and SnPb/Cu solder joints but along the solder/Cu interface for the SnBi/Cu solder joints. The mechanical properties of solder play important roles in the fatigue lives by influencing the crack initiation mechanism, while the interfacial microstructure determines the propagation cycles by dominating the fracture strength of solder joints.

(2) When the loading direction is parallel to the interfaces, the plastic deformation of the Cu substrate, solder and IMC layer
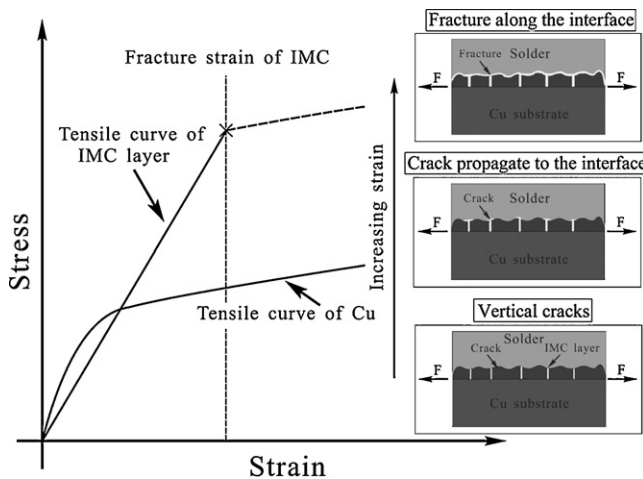

Fig. 11. Fatigue fracture mechanism and damage process of Cu/solder interface under parallel loading.

increase synchronously with increasing cyclic number, the local IMC layer fractures perpendicular to the IMC/Cu interface firstly when the cumulative strain exceeds its fracture strain. Then the cracks propagate into the solder/IMC interface, link up and induce fracture along the interface. The fracture strength (strain) of the interfacial IMC layer is the dominating factor of fatigue resistance in this case, while the mechanical properties of solders have little influence.

Acknowledgements

References

[1] IPC Roadmap: A Guide for Assembly of Lead-free Electronics, Draft IV, 2000.
[2] S.K. Kang, A.K. Sarkhel, J. Electron. Mater. 23 (1994) 701–707.
[3] M. Abtew, G. Selvaduray, Mater. Sci. Eng. R 27 (2000) 95–141.
[4] H.K. Kim, K.N. Tu, Appl. Phys. Lett. 67 (1995) 2002–2004.
[5] C. Anderssona, Z. Lai, J. Liu, H. Jiang, Y. Yu, Mater. Sci. Eng. A 394 (2005) 20–27.
[6] M.A. Matin, W.P. Vellinga, M.G.D. Geers, Mater. Sci. Eng. A 445–446 (2007) 73–85.
[7] J. Zhao, Y. Miyashita, Y. Mutoh, Int. J. Fract. 23 (2001) 723–731.
[8] J. Zhao, Y. Mutoh, Y. Miyashita, L. Wang, Eng. Fract. Mech. 70 (2003) 2187–2197.
[9] J. Zhao, Y. Mutoh, Y. Miyashita, S.L. Mannan, J. Electron. Mater. 31 (2002) 879–886.
[10] M. Erinc, T.M. Assman, P.J.G. Schreurs, M.G.D. Geers, Int. J. Fract. 152 (2008) 37–49.
[11] S.K.W. Seah, E.H. Wong, V.P.W. Shim, Scr. Mater. 59 (2008) 1239–1242.
[12] C. Kanchanomai, Y. Miyashita, Y. Mutoh, S.L. Mannan, Mater. Sci. Eng. A 345 (2003) 90–98.
[13] C. Kanchanomai, Y. Mutoh, Mater. Sci. Eng. A 381 (2001) 113–120.
[14] Q.S. Zhu, Z.F. Zhang, Z.G. Wang, J.K. Shang, J. Mater. Res. 23 (2008) 78–82.
[15] T.Y. Lee, W.J. Choi, K.N. Tu, J. Mater. Res. 17 (2002) 291–301.
[16] Q.K. Zhang, H.F. Zou, Z.F. Zhang, J. Electron. Mater. 38 (2009) 852–859.
[17] Q.S. Zhu, Z.F. Zhang, J.K. Shang, Z.G. Wang, Mater. Sci. Eng. A 435–436 (2006) 588–594.
[18] J.W. Evans, A Guide to Lead-free Solders, Springer, London, 2007, pp. 6–15.
[19] J.J. Sundelin, S.T. Nurmi, T.K. Lepisto, E.O. Ristolainen, Mater. Sci. Eng. A 420 (2006) 55–62.
[20] Z. Mei, J.W. Morris Jr., J. Electron. Mater. 21 (1992) 599–607.
[21] O. Fouassier, J.M. Heintz, J. Chazelas, P.M. Geffroy, J.F. Silvaina, J. Appl. Phys. 100 (2006) 043519.
[22] Y. Ding, C.Q. Wang, Y.H. Tian, M.Y. Li, J. Alloys Compd. 428 (2007) 274–285.
[23] P.L. Liu, J.K. Shang, J. Mater. Res. 16 (2001) 1651–1659.
[24] J. Glazer, Int. Mater. Rev. 40 (1995) 65–93.
[25] M. McCormack, S. Jin, G.W. Kammlott, H.S. Chen, Appl. Phys. Lett. 63 (1993) 15–17.
[26] C.J. Thwaites, Soft Soldering Handbook, International Tin Research Institute, Publication No. 533, 1977.
[27] H. Rack, J. Maurin, J. Test. Eval. 2 (1974) 351–353.
[28] S. Pattanaik, V. Raman, Proc. Mater. Dev. Microelec. Packg. Conf., ASM Intl., Materials Park, OH, 1991, p. 251.
[29] I. Shohji, T. Yoshida, T. Takahashi, S. Hioki, Mater. Sci. Eng. A 366 (2004) 50–55.
[30] M. Kerr, N. Chawla, Acta Mater. 52 (2004) 4527–4535.
[31] S. Vaynman, M.E. Fine, D.A. Jeannotte, Metall. Trans. A 19 (1988) 1051–1059.
[32] H.T. Lee, M.H. Chen, H.M. Jao, T.L. Liao, Mater. Sci. Eng. A 358 (2003) 134–141.
[33] Q.K. Zhang, Z.F. Zhang, J. Alloys Compd. 485 (2009) 853–861.
[34] Q.K. Zhang, H.F. Zou, Z.F. Zhang, J. Mater. Res., accepted.
[35] J. Glazer, J. Electron. Mater. 23 (1994) 693–700.
[36] C. Lea, A Scientific Guide to Surface Mount Technology, Electrochemical Publications Ltd., GB-Port Erin, British Isles, 1988.